Structural study of the pressure-induced metal-insulator transition in LiV_2O_4

Alexander J. Browne,[1] Edward J. Pace,[1] Gaston Garbarino,[2] and J. Paul Attfield[1,*]

[1]*Centre for Science at Extreme Conditions and School of Chemistry, University of Edinburgh, West Mains Road, Edinburgh EH9 3FD, United Kingdom*

[2]*ESRF, The European Synchrotron, 71 Avenue des Martyrs, 38000 Grenoble, France*

(Received 11 September 2019; published 21 January 2020)

At ambient pressure the spinel LiV_2O_4 is a metal with a heavy fermion ground state. However, under applied pressure a transition to an insulating, nonmagnetic state occurs. Powder x-ray diffraction has been used to study structural changes associated with this transition, and reveals that the ambient-pressure $Fd\bar{3}m$ spinel structure distorts to a monoclinic cell of $C2/m$, $C2$, or Cm symmetry above 11 GPa at low temperatures. The changes of structure and properties provide evidence for orbital molecule formation in the cubic phase at high pressures and low temperatures that leads to long-range orbital molecule order in the monoclinic phase.

DOI: 10.1103/PhysRevMaterials.4.015002

I. INTRODUCTION

Metal-insulator transitions often occur in systems with strongly correlated electrons and are highly sensitive to perturbations such as a change of temperature, chemical substitution, or the application of pressure [1]. At ambient pressure the spinel LiV_2O_4 is a metal and has been of considerable interest as it was the first d-electron system in which heavy-fermion mass enhancement was observed [2]. An initial high-pressure study of this material showed that, at 10 K, a transition to an insulating state is induced at 6.8 GPa [3]. Subsequent optical measurements revealed a pressure-temperature phase diagram with three distinct regions—a low-pressure metallic phase and a high-pressure insulating one with markedly different, pressure-independent conductivities, separated by an intermediate region in which the change from metallic to insulating conductivity gradually occurs [4]. The magnetic behavior of LiV_2O_4 under pressure has also been studied—^{7}Li- and ^{51}V-NMR have revealed that the local-moment low-pressure phase gradually converts to a spin-singlet high-pressure one, and that this conversion starts to occur at pressures consistent with the metallic-intermediate phase boundary determined by the optical measurements [5].

The high-pressure change in LiV_2O_4 is reminiscent of transitions exhibited by VO_2 and other vanadium oxides that are associated with the formation of orbital molecules—small clusters of transition metal cations formed by covalent d-d bonding [6,7]. In addition to changes of properties, which result from the localization and spin pairing of d electrons into V-V bonds, the formation of orbital molecules in these materials is associated with a structural distortion, as the distance between the bonded cations is typically shortened by several tenths of an Ångstrom. However, characterization of the structure of LiV_2O_4 under pressure is lacking. A distortion of the cubic $Fd\bar{3}m$ structure of the metallic phase was reported on the basis of powder x-ray diffraction results, though it was found to occur at a higher pressure—12.8 GPa at 10 K—than the change of resistivity reported concurrently [3]. From the observed peak splitting it was suggested that this high-pressure phase has an $R\bar{3}m$ symmetry superstructure similar to that of AlV_2O_4. At ambient pressure and high temperatures AlV_2O_4 adopts the cubic $Fd\bar{3}m$ spinel structure, but long-range charge and orbital ordering induces an $R\bar{3}m$ distortion of a $2 \times 2 \times 2$ cubic supercell to give a ground state structure in which pairs of V_3^{9+} and V_4^{8+} orbital molecules (originally thought to be V_7^{17+} heptamers) are found [8,9]. The isoelectronic material GaV_2O_4 behaves similarly [10]. The orbital molecules in the $R\bar{3}m$ structures of these materials are defined by short V-V distances, and an EXAFS study of LiV_2O_4 identified similar shortening above 12 GPa at 300 K [11]. To explore the structural changes further, we have carried out the high-pressure x-ray diffraction study reported here.

II. EXPERIMENT

Powder x-ray diffraction data were collected at beamline ID15B of the European Synchrotron Radiation Facility (ESRF). A polycrystalline sample of LiV_2O_4 was prepared by a high-temperature solid state reaction and portions were loaded into two identical symmetrical-type diamond anvil cells (DACs) prepared with 300 μm anvil culets and stainless-steel gaskets indented to 30 μm. Using helium as the pressure-transmitting medium, the pressure was controlled online using a gas membrane and calibrated using online ruby fluorescence [12]. One DAC was used for measurements at 300 K, with the pressure increased to 21.0 GPa before the gasket failed. The second DAC was cooled to 20 K using a He cryostat and a first set of measurements were made at this temperature upon compression to 15.3 GPa. The DAC was then warmed to 100 K with pressure maintained and a second set of measurements were made upon decompression from 15.5 GPa at this higher temperature. The diffraction pattern at each pressure-temperature step was recorded on a Mar555 2D detector using a 1 s exposure of 30 keV radiation ($\lambda = 0.411536$ Å), during which the DAC was rocked by $\pm 3^\circ$.

*Corresponding author: j.p.attfield@ed.ac.uk

The collected diffraction patterns were processed using DIOPTAS [13]. The intensities and profiles of the measured Bragg reflections were found to be strongly affected by texturing and strain effects, preventing meaningful Rietveld refinement of the structure from being carried out, although the lattice parameters of the unit cell could be determined through Le Bail fitting done using GSAS [14]. The region $2\theta = 6.0^\circ - 7.8^\circ$ was excluded from all fits to mask a broad background feature. This feature is relatively weak [maximum intensity 15 arb. units on the scale shown on Fig. 2(b)] and it was clear that no significant Bragg intensities were observed in this region.

III. RESULTS

At ambient pressure, LiV_2O_4 has a cubic $Fd\bar{3}m$ normal spinel structure down to the lowest temperatures [15]. Our diffraction patterns show that this structure also remains undistorted over the whole range of pressures measured at 300 K [Figs. 1(a) and 1(b)]. This reveals that the structural response of LiV_2O_4 to pressure varies with length scale, as while we do not find a long-range crystallographic distortion below 21.0 GPa at 300 K EXAFS has revealed a local-structure distortion at 12 GPa at this temperature [11].

The refined volume of the $Fd\bar{3}m$ unit cell decreases smoothly with pressure and can be fit with the second-order Birch-Murnaghan equation of states [16], with $V_0 = 560.2(2)$ Å^3 and $B_0 = 123.2(6)$ GPa [Fig. 1(c)]. This value of V_0 corresponds to cubic lattice parameter $a_C = 8.244$ Å, consistent with previously reported values [15]. The bulk modulus B_0 is smaller than the 160–180 GPa values measured for AV_2O_4 vanadium oxide spinels with divalent A-site cations [17], likely due to the greater compressibility of monovalent Li^+.

A previous high-pressure diffraction study of LiV_2O_4 reported a distortion of the crystal structure above 12.8 GPa at 10 K [3]. Our 20 and 100 K data show clear evidence of a phase transition at 12.1 GPa and higher pressures [Fig. 2(a)]. An apparent small splitting of the cubic-(551) reflection at $2\theta = 20.9^\circ$ is observed in the 6.6 GPa data shown in the right-hand panel of Fig. 2(a). However, this is attributed to nonhydrostatic pressure effects as no other peak splittings are observed at this pressure, and the apparent splitting is not present in the 9.2 GPa data. The high pressure phase of LiV_2O_4 was previously suggested to have $R\bar{3}m$ symmetry, similar to the distortion that occurs in AlV_2O_4 at ambient pressure [8]. In the diffraction patterns we collected at 20 and 100 K, the proposed $R\bar{3}m$ symmetry does not account for all of the observed reflections [Fig. 2(a)]. Instead, a monoclinically distorted $R\bar{3}m$ unit cell, described as having $C2/m$ space group symmetry in the Le Bail fits although $C2$ and Cm symmetries are also possible, is required to index the observed reflections [Fig. 2(b)]. The metrically cubic lattice parameters of this monoclinic unit cell are $a_M = \sqrt{1.5}a_C$, $b_M = c_M = a_C/\sqrt{2}$, and $\beta = 125.26^\circ$, and its volume is half that of the cubic cell: $V_M = V_C/2$. Fits using other structural symmetries, or a mix of cubic and rhombohedral phases, give poorer agreement with the data [Fig. 2(c)]. Therefore, Le Bail fits of either a $Fd\bar{3}m$ or a $C2/m$ unit cell were made to all of the diffraction patterns collected at 20 and 100 K, and these

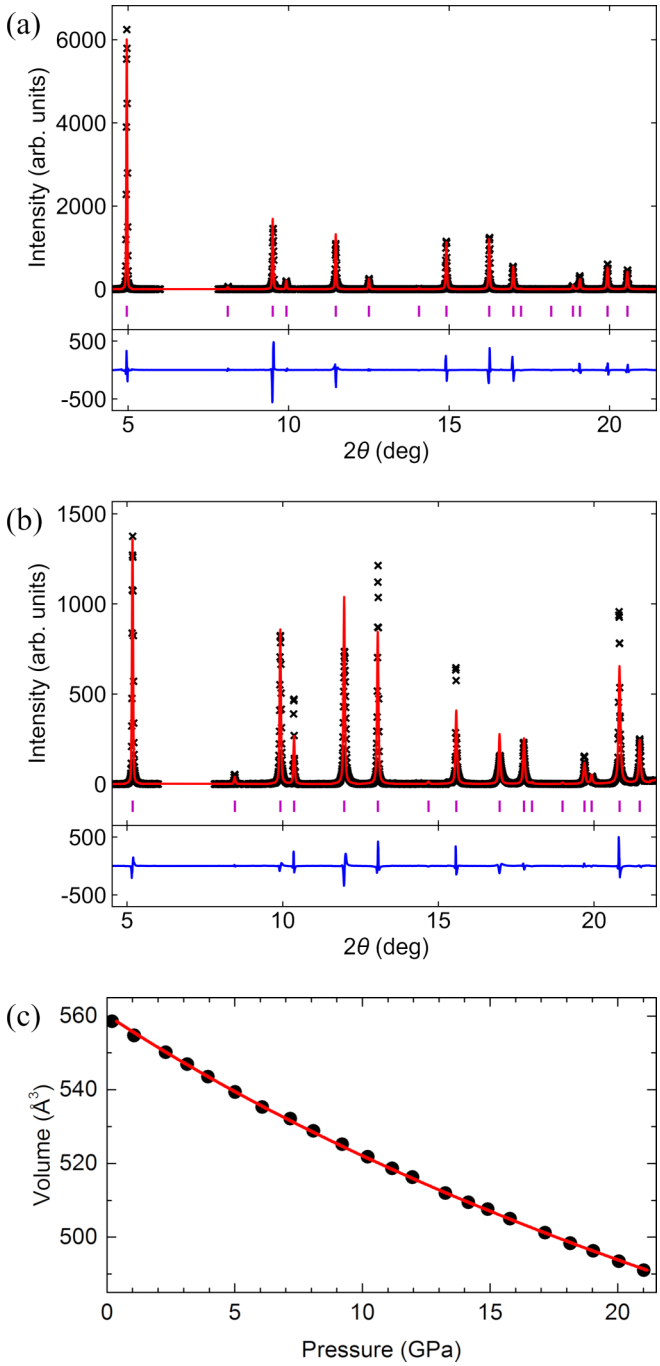

FIG. 1. Le Bail fits of an $Fd\bar{3}m$ unit cell to the 300 K diffraction patterns of LiV_2O_4 at (a) 0.2 GPa ($R_{wp} = 26.3\%$, $\chi^2 = 3.29$) and (b) 21.0 GPa ($R_{wp} = 35.6\%$, $\chi^2 = 4.28$). Although the Bragg profiles are affected by texturing and strain at high pressure, no peak splitting occurs. (c) Fit of the Birch-Murnaghan equation of states to the refined volumes of the $Fd\bar{3}m$ unit cell at 300 K.

determine that the transition between these two phases occurs at 11 GPa at 20 K and 12 GPa at 100 K as shown in Fig. 3. Fits of the Birch-Murnaghan equation of states to the values of V_C and $2V_M$ obtained at 20 K give $V_0 = 558.0(1)$ Å^3 and $B_0 = 139.6(9)$ GPa for the $Fd\bar{3}m$ phase, and $V_0 = 555.6(8)$ Å^3 and $B_0 = 123(2)$ GPa for the monoclinic phase. From these values, a volume decrease of 1.25% at the phase transition can be

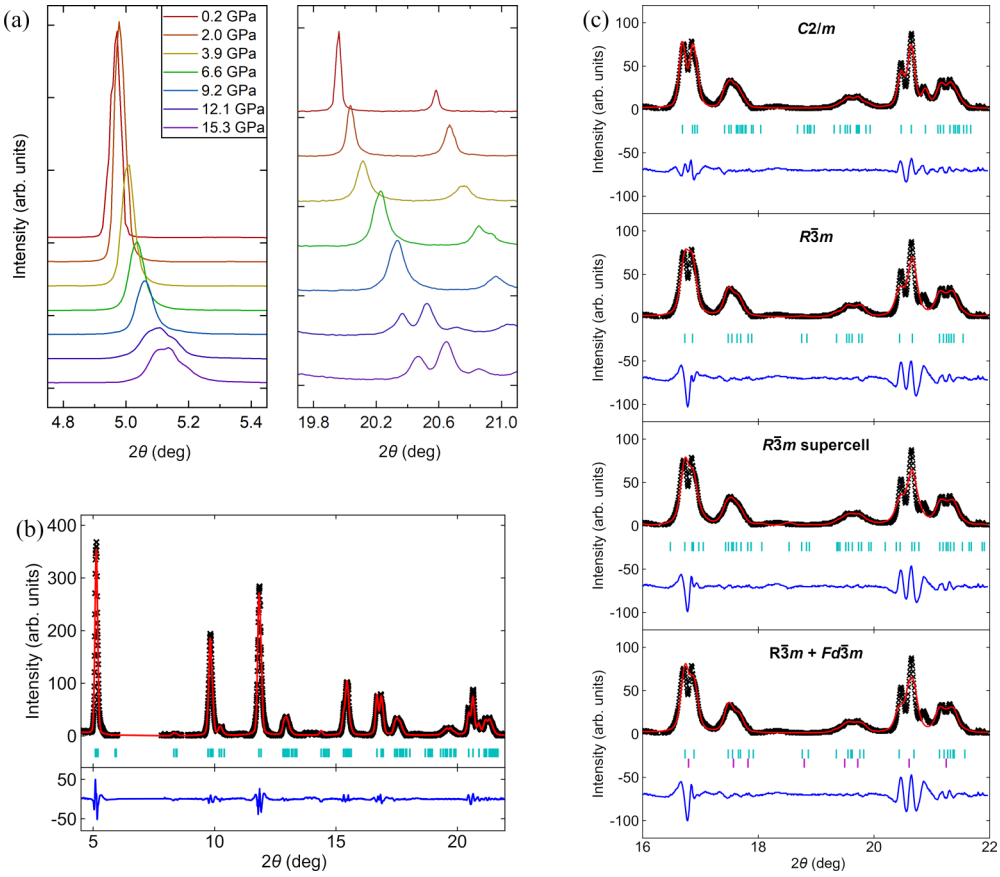

FIG. 2. (a) Diffraction patterns collected at 20 K reveal that the 111 ($2\theta = 4.97^\circ$ at 0.2 GPa) and 444 ($2\theta = 19.96^\circ$ at 0.2 GPa) Bragg peaks of the $Fd\bar{3}m$ structure each split into three at high pressure. For the suggested $R\bar{3}m$ distortion [3] these peaks should only split into two. (b) Le Bail fit of a monoclinic $C2/m$ unit cell to the diffraction pattern of LiV_2O_4 at 20 K and 15.3 GPa ($R_{wp} = 22.0\%$, $\chi^2 = 0.94$). (c) Comparison of the high-angle region of the fit in (b) to those of fits of $R\bar{3}m$ ($R_{wp} = 27.6\%$, $\chi^2 = 1.47$), AlV_2O_4-like $R\bar{3}m$-supercell ($R_{wp} = 26.1\%$, $\chi^2 = 1.32$), and coexisting $R\bar{3}m$ and $Fd\bar{3}m$ ($R_{wp} = 25.9\%$, $\chi^2 = 1.30$) unit cells.

determined. A pressure-induced softening of the lattice is also notable, as B_0 decreases by 12% through the transition. This is consistent with the orbital molecule formation described below, as this leads to weakening of the V-V interactions between the bonded clusters so the lattice softens.

In the $Fd\bar{3}m$ structure of LiV_2O_4, each V cation has six equidistant V nearest neighbors. From the Birch-Murnaghan fit to V_C at 20 K this $Fd\bar{3}m$ phase is predicted to have a lattice parameter $a_C = 7.99$ Å at 15.3 GPa, corresponding to a V-V nearest-neighbor distance of 2.82 Å if it was to remain undistorted, though LiV_2O_4 actually adopts a $C2/m$ or lower symmetry monoclinic structure under these conditions. In this structure there are three V crystallographic sites (Table I) and four distinct V-V nearest-neighbor distances that become inequivalent under the monoclinic lattice distortion, even if the V atoms remain at their $Fd\bar{3}m$-cell coordinates. From the 20 K–15.3 GPa Le Bail fit [Fig. 2(b)] refined lattice parameters $a_M = 9.8552(8)$ Å, $b_M = 5.6128(5)$ Å, $c_M = 5.6004(7)$ Å, and $\beta = 125.844(6)^\circ$ are obtained, for which the V-V distances with the V atoms at their $Fd\bar{3}m$-cell coordinates are 2.7929(3) Å (V1−V2 × 2), 2.8002(4) Å (V1–V3), 2.8064(2) Å (V2–V2), and 2.8354(2) Å (V2−V3 × 2). Four of these six distances are shorter than that predicted for the cubic phase under the same conditions.

Shortening of metal-metal distances is the signature of orbital molecule formation [7]. Many vanadium oxides have orbital molecule ground states—$(V^{4+})_2$ dimers form in VO_2 below the Peierls transition [18] and in V_4O_7 [19], while $(V^{3+})_3$ trimers are found in $LiVO_2$ [20] and $BaV_{10}O_{15}$ [21], and $(V^{3+})_3$ trimers and $(V^{2+})_4$ tetramers coexist in AlV_2O_4 [9] and GaV_2O_4 [10]. In all of these materials, the orbital molecules emerge through an ordering transition where the lattice distorts and a change of symmetry allows ordered displacements of the V atoms. The V-V nearest-neighbor distances in the ground states of VO_2 ($P4_2/mnm$ to $P2_1/c$, $T_{MI} = 340$ K), $LiVO_2$ ($R\bar{3}m$ to $3 \times 3 \times 1$ $R\bar{3}m$ supercell, $T_{MI} \approx 450$ K) and AlV_2O_4 ($Fd\bar{3}m$ to $R\bar{3}m$, $T_{CO} = 700$ K) are compared in Table II. For each material, two sets of V-V distances are given—"undisplaced" values calculated from the unit cell parameters (i.e., assuming that atoms remain at the same coordinates as in the high-temperature structure after transformation to the low-temperature cell setting), and the experimentally determined "displaced" values that result from the lattice distortion and the refined vanadium coordinate shifts. The displaced values show a much greater dispersion between short and long V-V distances, which are respectively those within and between the orbital molecules.

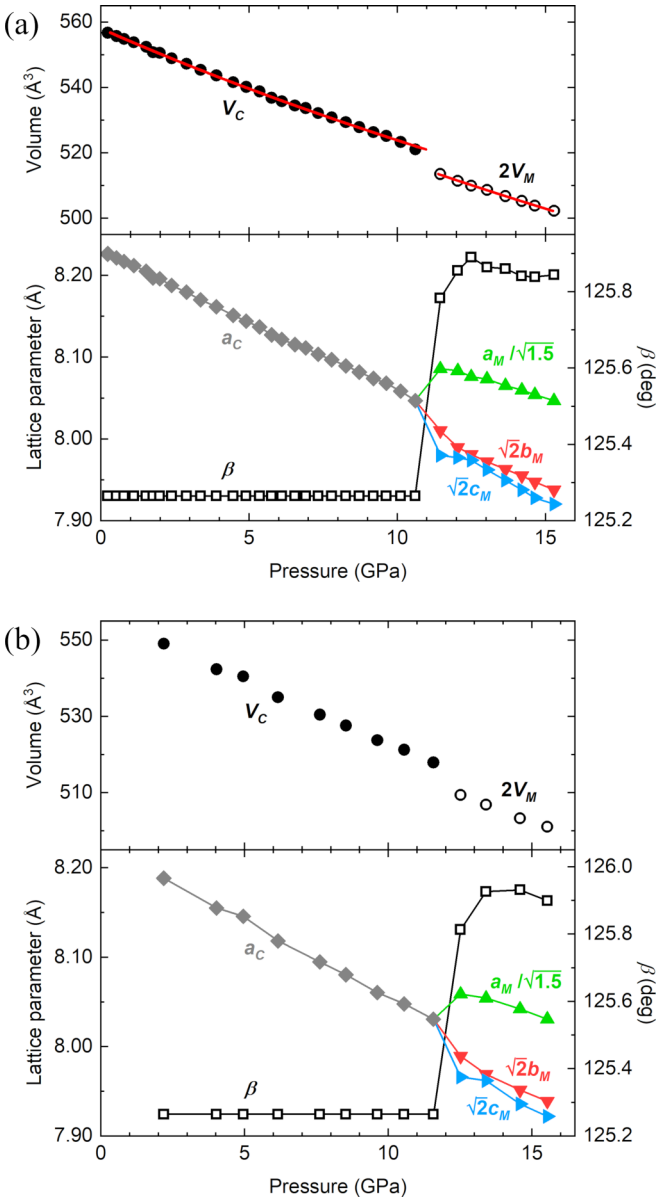

FIG. 3. Refined cell parameters of LiV_2O_4 at (a) 20 K and (b) 100 K, obtained from Le Bail fits of $Fd\bar{3}m$ and $C2/m$ unit cells. The transition between these two phases occurs at 11 GPa for 20 K, and at 12 GPa for 100 K. Fits of the Birch-Murnaghan equation of states to the unit cell volumes of the two phases at 20 K are shown.

For LiV_2O_4, both the range of undisplaced V-V distances calculated from the monoclinic cell parameters at 20 K and 15.3 GPa and the range of displaced distances from a previous EXAFS analysis at 21.7 GPa and 300 K [11] are comparable

TABLE I. Wyckoff positions and transformed $Fd\bar{3}m$-cell coordinates of the vanadium sites in the monoclinic $C2/m$ cell of LiV_2O_4.

Site	Wyck.	x	y	z
V1	2*d*	0	0.5	0.5
V2	4*e*	0.25	0.25	0
V3	2*b*	0	0.5	0

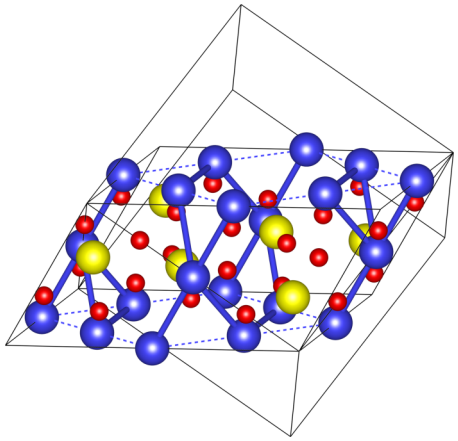

FIG. 4. $C2/m$ unit cell of the high-pressure monoclinic phase of LiV_2O_4, shown in relation to the $Fd\bar{3}m$ unit cell of the low-pressure phase. All atoms in the monoclinic cell are shown (yellow = Li, blue = V, red = O), at their $Fd\bar{3}m$-cell positions. For the V sublattice this means that all V-V nearest-neighbor distances are equivalent; however, the monoclinic distortion breaks this equivalence, and the distances that become shorter and longer than the cubic one are shown as solid and dashed bonds, respectively.

to those for the orbital molecule vanadium oxides in Table II. $C2/m$ symmetry fixes the V atoms at their undisplaced sites, but $C2$ or Cm symmetry gives them some variable coordinates that permit movement to displaced positions. Hence it is highly likely that the low-temperature, high-pressure insulating phase of LiV_2O_4 has an orbital molecule ground state with $C2$ or Cm space group symmetry. In a charge-ordered $LiV^{3+}V^{4+}O_4$ insulator, up to two and one V-V bonds are

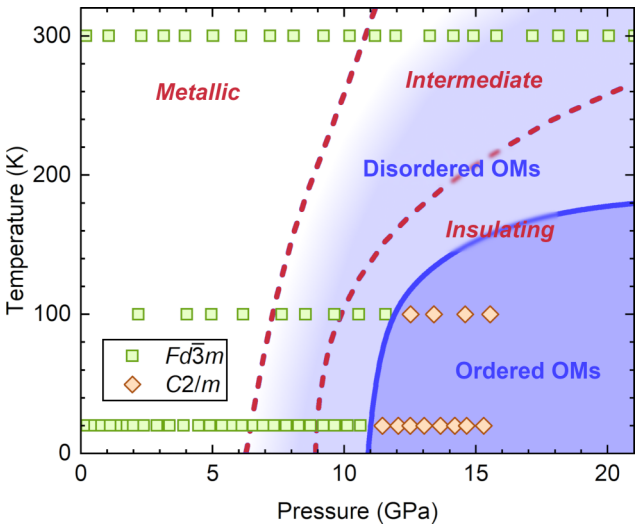

FIG. 5. Pressure-temperature phase diagram of LiV_2O_4. The solid line demarcates the $Fd\bar{3}m$ and $C2/m$ phases that we have observed, while the dashed lines follow the boundaries between regions of metallic, intermediate, and insulating behavior previously determined by optical measurements [4]. These likely correspond to regions where V-V bonding is, respectively, absent, partial and saturated, while the orbital molecules (OMs) formed by this bonding become ordered through the transition to the monoclinic phase.

TABLE II. Comparison of V-V nearest-neighbor distances (in Å) in the orbital molecule ground states of VO_2, $LiVO_2$, and AlV_2O_4 to those found in the monoclinic phase of LiV_2O_4. For each material, the undisplaced column lists the V-V distances that are calculated from the low-temperature unit cell parameters without any displacements of the atomic sites, while the displaced column lists the distances from the refined crystal structures, when available, which also include atom displacements. The low-temperature crystal structure of LiV_2O_4 could not be refined here but the range of displaced distances determined by a previous EXAFS study [11] is similar to the dispersion of V-V distances in the other orbital molecule examples.

VO_2		$LiVO_2$		AlV_2O_4		LiV_2O_4	
Undisplaced	Displaced	Undisplaced	Displaced	Undisplaced	Displaced	Undisplaced	Displaced
293 K [18]		300 K [20]		300 K [9]		20 K, 15.3 GPa [This work]	300 K, 21.7 GPa [11]
					2.61	2.79	
2.88	2.60	2.83	2.54	2.88	2.62	2.80	2.66–3.08
	3.19		3.00	2.92	3.01	2.81	
					3.04	2.84	
					3.14		

expected per V^{4+} (d^1) and V^{3+} (d^2), respectively, according to simple valence bond rules, so V atom displacements are expected to lead to the shortening of a subset of the short undisplaced V-V distances within the monoclinic unit cell shown in Fig. 4.

IV. DISCUSSION

The pressures at which we have observed the $Fd\bar{3}m$ to monoclinic crystallographic distortion in LiV_2O_4, 11 GPa at 20 K and 12 GPa at 100 K, are close to that of 12.8 GPa at 10 K at which a distortion in this material had previously been reported [3]. However, as shown in Fig. 5, the structural phase boundary lies to higher pressures and lower temperatures than the previously reported boundary between the regions of intermediate and insulating behavior. The pressures at which the resistivity and magnetism of LiV_2O_4 have been reported to change [3,5], as well as the local-structure distortion identified by EXAFS [11], seem to coincide with the metallic-intermediate boundary. It was suggested that the intermediate region of the phase diagram exists because the transition between the metallic and insulating phases occurs gradually, through the development of insulating grains [5]. However, no coexistence of cubic and monoclinic phases is observed in the intermediate region in our study, and instead a complete conversion between the cubic and monoclinic phases occurs abruptly at the determined pressures. A more likely explanation is that orbital molecules are formed locally through electron localization in the intermediate region, but without their long-range order.

The metallic-intermediate boundary for LiV_2O_4—at which the local structure distorts and the electronic properties of the material start to change on pressurization—indicates the pressure at which strong electron-electron correlations start to lead to charge localization and the emergence of local V-V bonding interactions. As the pressure is increased through the intermediate region more and more cations form bonds with their neighbors, hence the gradual conversion from metallic and local moment to insulating and spin-singlet behavior in this region. At the intermediate-metallic boundary—above which the electronic properties do not change with further increases of pressure—pairing of valence d electrons in V-V bonds is likely complete. Long-range order of the orbital molecules occurs at a still higher pressure, through the transition between $Fd\bar{3}m$ and $C2/m$ (or more likely $C2$ or Cm) structures that we have observed. A strong precedent for the formation of disordered orbital molecules in the cubic spinel phase of LiV_2O_4 approaching the monoclinic phase boundary is provided by AlV_2O_4 and GaV_2O_4, in which disordered orbital molecules have been evidenced up to 1100 K, well above the structural transitions (at 700 and 450 K, respectively) below which long range orbital molecule order is observed [9,10]. In addition, local, disordered trimeron orbital molecules have been evidenced up to the 850 K Curie point in the spinel magnetite Fe_3O_4, far above the electronic ordering (Verwey) transition at 125 K [22]. Further high-pressure crystallographic studies will be needed to determine the space group and full monoclinic structure of LiV_2O_4, and hence to confirm the presence and nature of the expected orbital molecules.

ACKNOWLEDGMENTS

Financial support for this work was provided by the European Research Council (ERC) (Advanced Grant EC339312), and access to the European Synchrotron Radiation Facility (ESRF) was supported by the Science and Technology Facilities Council (STFC).

[1] M. Imada, A. Fujimori, and Y. Tokura, Rev. Mod. Phys. **70**, 1039 (1998).

[2] S. Kondo, D. C. Johnston, C. A. Swenson, F. Borsa, A. V. Mahajan, L. L. Miller, T. Gu, A. I. Goldman, M. B. Maple, D. A. Gajewski, E. J. Freeman, N. R. Dilley, R. P. Dickey, J. Merrin, K. Kojima, G. M. Luke, Y. J. Uemura, O. Chmaissem, and J. D. Jorgensen, Phys. Rev. Lett. **78**, 3729 (1997).

[3] K. Takeda, H. Hidaka, H. Kotegawa, T. Kobayashi, K. Shimizu, H. Harima, K. Fujiwara, K. Miyoshi, J. Takeuchi, Y. Ohishi, T. Adachi, M. Takata, E. Nishibori, M. Sakata, T. Watanuki, and O. Shimomura, Physica B: Condens. Matter **359**, 1312 (2005).

[4] A. Irizawa, S. Suga, G. Isoyama, K. Shimai, K. Sato, K. Iizuka, T. Nanba, A. Higashiya, S. Niitaka, and H. Takagi, Phys. Rev. B **84**, 235116 (2011).
[5] H. Takeda, Y. Kato, M. Yoshimura, Y. Shimizu, M. Itoh, S. Niitaka, and H. Takagi, Phys. Rev. B **92**, 045103 (2015).
[6] J. B. Goodenough, J. Solid State Chem. **3**, 490 (1971).
[7] J. P. Attfield, APL Mater. **3**, 041510 (2015).
[8] K. Matsuno, T. Katsufuji, S. Mori, Y. Moritomo, A. Machida, E. Nishibori, M. Takata, M. Sakata, N. Yamamoto, and H. Takagi, J. Phys. Soc. Jpn. **70**, 1456 (2001).
[9] A. J. Browne, S. A. J. Kimber, and J. P. Attfield, Phys. Rev. Mater. **1**, 052003(R) (2017).
[10] A. J. Browne, C. Lithgow, S. A. J. Kimber, and J. P. Attfield, Inorg. Chem. **57**, 2815 (2018).
[11] L. Pinsard-Gaudart, N. Dragoe, P. Lagarde, A. M. Flank, J. P. Itie, A. Congeduti, P. Roy, S. Niitaka, and H. Takagi, Phys. Rev. B **76**, 045119 (2007).
[12] H. K. Mao, J. Xu, and P. M. Bell, J. Geophys. Res. **91**, 4673 (1986).
[13] C. Prescher and V. B. Prakapenka, High Press. Res. **35**, 223 (2015).
[14] A. C. Larson and R. B. Von Dreele, Los Alamos National Laboratory Report LAUR 86-748, 2004.
[15] O. Chmaissem, J. D. Jorgensen, S. Kondo, and D. C. Johnston, Phys. Rev. Lett. **79**, 4866 (1997).
[16] F. Birch, Phys. Rev. **71**, 809 (1947).
[17] Z.-Y. Li, X. Li, J.-G. Cheng, L. G. Marshall, X.-Y. Li, A. M. dos Santos, W.-G. Yang, J. J. Wu, J.-F. Lin, G. Henkelman, T. Okada, Y. Uwatoko, H. B. Cao, H. D. Zhou, J. B. Goodenough, and J.-S. Zhou, Phys. Rev. B **94**, 165159 (2016).
[18] K. D. Rogers, Powder Diffraction **8**, 240 (1993).
[19] M. Marezio, D. B. McWhan, P. D. Dernier, and J. P. Remeika, J. Solid State Chem. **6**, 419 (1973).
[20] F. Pourpoint, X. Hua, D. S. Middlemiss, P. Adamson, D. Wang, P. G. Bruce, and C. P. Grey, Chem. Mater. **24**, 2880 (2012).
[21] T. Kajita, T. Kanzaki, T. Suzuki, J. E. Kim, K. Kato, M. Takata, and T. Katsufuji, Phys. Rev. B **81**, 060405(R) (2010).
[22] G. Perversi, E. Pachoud, J. Cumby, J. M. Hudspeth, J. P. Wright, S. A. J. Kimber, and J. P. Attfield, Nat. Commun. **10**, 2857 (2019).